Available online at BCREC website: https://bcrec.id

Bulletin of Chemical Reaction Engineering & Catalysis, 15 (2) 2020, 304-318

Research Article

Synergistic Effect of Microwave Calcination and Sonophotocatalytic Activity of TiO_2-Montmorillonite on The Degradation of Direct Yellow 106 and Disperse Violet 1

Issma Labib, Hocine Boutoumi*, Hussein Khalaf

Laboratoire de Génie Chimique (LGC), Faculté de Technologie, Université Blida 1, B.P 270, Route de Soumaa, 09000 Blida, Algeria

Received: 5th January 2020; Revised: 26th February 2020; Accepted: 27th February 2020; Available online: 30th July 2020; Published regularly: August 2020

Abstract

The TiO_2-pillared montmorillonite nanoparticles (TiO_2-Mt) were prepared by the sol-gel method, then applied for the elimination of dyes in solution: CI Direct Yellow 106 (DY106) (azo dye) and CI Disperse Violet 1 (DV1) (anthraquinone dye) by the sonocatalytic, photocatalytic and sonophotocatalytic processes, in order to test the efficiency of photocatalysts, while photolysis, sonolysis, and sonophotolysis tests have been done previously. The photocatalysts (TiO_2-Mt) were characterized by X-ray Diffraction (XRD), X-ray Fluorescence analysis (XRF), Brunauer-Emmet-Teller (BET), Scanning Electron Microscopy (SEM) methods, thermal and thermogravimetric analysis (TG/DTA) and the zero load point (pH_{pzc}). Aqueous solutions of dye of an initial concentration (50 mg/L), in the presence of 1 g/L of photocatalyst, were irradiated using a mercury lamp (Hg) of 40 Mw/cm^2 and put in contact with an ultrasonic probe with a frequency of 20 kHz and a power of 750 W, providing the ultrasound. The results obtained indicate that a weak, good and better dye degradation rate has been observed successively by the application of the sonocatalytic, photocatalytic, and sonophotocatalytic processes, where the latter has shown a synergistic effect, while the photocatalyst TiO_2-Mt/MW showed significant efficiency during the degradation, due to the beneficial effect of the microwave calcination mode.

Keywords: TiO_2-Montmorillonite; Microwave calcinations; Sonophotocatalysis; Direct Yellow 106; Disperse Violet 1

How to Cite: Labib, I., Boutoumi, H., Khalaf, H. (2020). Synergistic Effect of Microwave Calcination and Sonophotocatalytic Activity of TiO_2-Montmorillonite on The Degradation of Direct Yellow 106 and Disperse Violet 1. *Bulletin of Chemical Reaction Engineering & Catalysis*, 15(2), 304-318 (doi:10.9767/bcrec.15.2.6999.304-318)

Permalink/DOI: https://doi.org/10.9767/bcrec.15.2.6999.304-318

1. Introduction

Environmental pollution has become a major concern due to municipal and industrial discharges. The elimination of these requires effective and profitable solutions, especially in the case of industrial effluents containing various toxic organic compounds [1].

The textile industry is known as one of the largest industries consuming water and contributes to the discharge of wastewater into watercourses [2], containing mainly colored solutions, which harm aquatic life, ecosystem and human health (contamination of drinking water supplies), due to their variety, toxicity and resistance to treatment [3].

At very low concentrations of dyes, the color of the effluents is visually identifiable. This pol-

* Corresponding Author.
E-mail: ybentoumi@ymail.com (H. Boutoumi)

lution prevents the penetration of light and thus reduces the photosynthesis of aquatic plants and affects their growth. Depending on their chemical structure and the type of chromosphere, 20 to 30 types of dyes are used in the textile industry [4], 700,000 tones of 100,000 types of dyes are produced worldwide every year, while 1 to 15% of them are found in watercourses [5]. The three main families frequently used are phthalocyanine, anthraquinone and azo dyes. In the first position are the azo dyes (60% of the reactive dyes), followed by the anthraquinone dyes [6].

The treatment of colored water is a necessity to preserve environment and conventional methods, such as: filtration, sedimentation, adsorption, and coagulation alone, do not bring encouraging results to the elimination of dyes [7,8]. Unfortunately, pollution passes to another phase, thus leading to new dangerous products released into the environment [9].

Due to the high cost of treatments, intensive research has been carried out to develop new techniques for the treatment of textile waste [10], new high-reliability processes have emerged in recent years, called advanced oxidation processes (AOP), which lead to the mineralization of polluted water [11-13], among them, ultrasound are easy to use and very effective without creating new pollutants [14,15], but its application alone in the degradation of colored solutions is ineffective, whereas they are once combined with other AOPs [8], such as: sonophotocatalytic oxidation, ultrasound/H_2O_2, UV/H_2O_2, ultrasound/ozone, UV/ozone and the photo-Fenton process [16].

Some studies have shown a synergistic effect between photocatalysis coupled to ultrasound, confirmed by the reaction rate constant of the sonophotocatalytic process, which was greater than the sum of the two individual processes [17], thus proving its effectiveness as a method of treating polluted toxic water [18], demonstrating the role of OH• entities during degradation.

Additional OH•s are provided by acoustic ultrasonic cavitation, the latter can eliminate the intermediaries of the active photocatalytic sites, generates the shear forces, the turbulence and the micro-diffusion, which contribute to the regeneration of the active catalytic surface. They also increase the uniformity of the dispersion as well as the surface, when the catalyst or the pollutant are in the form of powder or agglomerate. It is also capable of improving mass transfer towards the liquid-solid interface and accelerates the adsorption activity of the reagent on the photocatalyst [19].

The degradation reaction is initiated by the OH• hydroxyl radicals formed through the combination of an h^+ hole with water adsorbed by electron transfer by photo-oxidation.

1st case: addition of the OH• radical on the organic compound R:

$$R + OH\bullet \rightarrow (ROH\bullet) \rightarrow hydroxylated\ products \quad (1)$$

2nd case: elimination of a hydrogen atom

$$RH_2 + OH\bullet \rightarrow (RH\bullet) + H_2O \rightarrow oxidized\ products \quad (2)$$

Reaction, accompanied by the cleavage of the dye molecule into two or more fragments at the level of a carbon-carbon bond. In recent years, various semiconductors have been studied as sonophotocatalysts by different research groups, such as: TiO_2 [20-25], Ag/TiO_2 [26], ZnO [27], Cu/ZnO [28], and CuO [29]. However, suspended particles create problems; their separation after use in water treatment is one of the difficulties encountered [30]. The TiO_2 is the most widely used semiconductor, due to its physical and chemical stability, as well as its low cost [31,32], while its use in large-scale industrial applications has been limited, due to its tendency to accumulate, thus creating problems of blockage like dysfunction [33]. On the other hand, the efficiency of the degradation process by TiO_2 is limited because the UV radiation absorbed by the latter represents only 5 % of the solar spectrum [34].

However, to overcome the recovery problem, the TiO_2 is supported on thin films or minerals [35], such as: pillared interlayer clay (named interlayer titanium clay), which is a laminated structure nanocomposite material with additional characteristics [36], for example, their large surface area, their large cation exchange capacities and their layered structure [31]. Montmorillonite is a widely used mineral clay, transformed into a rigid microporous material by fixing its pillars by calcination. Between the layers of this clay, the substitution of the cations Si(IV) by Al(III) and Al(III) by Mg(II) gives the network a negative charge balanced by the cations Na(I) and Ca(II). These cations can be replaced by oligomers of hydroxyl-metal cations which act as pillars separating the layers of the network [37]. The contact between TiO_2 and pollutants is improved in the case of natural clay with the TiO_2 pillar, due to its high photocatalytic activity and its good adsorption compared to pure TiO_2 [38].

The aim of the present study was to prepare TiO_2-pillared clay nanoparticles, to characterize the catalyst by X-ray Diffraction (XRD), X-ray Fluorescence (XRF), Scanning Electron Microscopy (SEM), Brunauer-Emmet-Teller methods (BET), thermal and thermogravimetric analysis (TG/DTA), and the zero charge point (pH_{PZC}), as well as its application as a heterogeneous photocatalyst, sonocatalyst, and sonophotocatalyst for effective degradation of the two dyes: C.I. Direct Yellow 106 (DY106) (azo dye)) and C.I. Disperse Violet 1 (DV1).

2. Materials and Methods

2.1 Materials

A bentonite from the (Maghnia-Algeria) Roussel deposit was used. TiO_2-P25 originated from Degussa (80% anatase, 20% rutile, nonporous). The titanium (IV) isopropoxide (97%) was purchased from Sigma-Aldrich. HCl was purchased from Cheminova and NaCl was from Panrea. The two dyes (azo and anthraquinone) were supplied by Boufarik textile industry (Algeria), purchased from Ciba-Geigy and used without further purification. The specifications of Direct Yellow 106 and Disperse Violet 1 are summarized in Table 1.

2.2 Preparation of TiO_2-Mt

The TiO_2-Mt photocatalyst was prepared by the sol-gel method, as mentioned in previous work by our team [39,40]. First of all, the raw bentonite was purified. It consisted in the removal of impurities, such as: calcite, sand, and feldspar. An amount of bentonite was dispersed in 1 M NaCl solution, in order to transform it to homoionic sodium form. Na-Mt was obtained by centrifugation of the fine particles (< 2 μm) recovered by siphonzation, while the residual chloride ions were removed by dialysis.

The montmorillonite suspension obtained with a molar ratio of 4 for HCl/Ti and 10 for a Ti/Na-Mt, was maintained at 50 °C with stirring for 3 h and then washed several times with distilled water by centrifugation. Thus the solid obtained was calcined at 400 °C for 3 h in an oven, or for 10 min in a commercial microwave oven at 800 W powers.

Table 1. Characteristics of DY106 and DV1 dyes.

Dyes	Molecular formula	λ_{max} (nm)
DY106	$C_{48}H_{26}N_8Na_6O_{18}S_6$	403
DV1	$C_{14}H_{10}N_2O_2$	534

2.3 Characterizations

The XRD spectrum of the raw bentonite, modified clay and the synthesized TiO_2-Mt nanocomposites was obtained using a X-ray diffractometer (D Philips: PW1800) with Cu-Kα radiation (λ = 1.5418 Å), 45 kV, 40 mA and at a scan rate of 0.02 °/s in the region of (0 - 50) 2θ. The basal spacing (d) was calculated from the (001) reflection via the Bragg equation ($\lambda = 2d \sin \theta$). The chemical composition was determined by X-ray fluorescence (XRF), using EPSILON 3 SERIES (PANalytical). A scanning electron microscopy (SEM) model JEOL.JEM-6360, controlled by a computer, used to detect the morphology of the samples. The measurement of the specific surface was made according to the method B.E.T (Brunauer, Emmet and Teller), by adsorbing liquid nitrogen at 77.3 K, by using a Micromeritics ASAP 2010 apparatus. The samples were degassed for about 24 hours at 200 °C under vacuum. Simultaneous Thermogravimetric Analyses (TG-DTA) were carried out using a SETARAM Labsys™ TG-DTA 12 instrument. However, the samples were heated from room temperature to 1200 °C, with a heating rate of 10 °C/min.

The point of zero charge (pH_{pzc}) of the photocatalysts was determined as follows: about 60 ml of NaCl solution (0.01 M) was introduced into erlenmeyer flasks and the pH was adjusted to 3, 4, 5, 6, 7, 8, 9, 10, and 11 using the solutions of HCl (0.1 M) and NaOH (0.1 M). The flasks were shaken in a shaker (Edmund Buhler GmbH SM-30) at 150 rpm and 25 °C for 48 h, after the addition of 0.2 g of the TiO_2-Mt nanoparticles. The final pH of each suspension was measured and plotted against the initial pH [31].

2.4 Adsorption Experiments

The experiments were carried out with a concentration of 50 mg/L of the DY106 and DV1 dyes, at pH of 6.3 and 1 g/L concentration of the two photocatalysts: TiO_2-Mt/MW and TiO_2-Mt/oven. Samples were withdrawn at regular intervals of time, centrifuged at 5000 rpm for 10 min and analyzed on a Shimadzu UV-1800 UV-Visible double beam spectrophotometer to determine the dye concentration, at the maximum wavelength of the absorption 534 nm and 403 nm for DY106 and DV1 dyes, respectively.

2.5 Photolysis, Sonolysis, Sonophotolysis, Photocatalysis, Sonocatalysis and Sonophotocatalysis Experiments

All experiments were carried out in a cylindrical glass reactor of 500 mL and equipped with a jacket, allowing the circulation of water to maintain the temperature at 19±1 °C. The source of UV radiations was produced by a 125 W Hg lamp, which has 40 Mw/cm^2 value of energy, measured by using a radiometer VLX-3W Digital mounted above the lamp at the same position as the photoreactor, corresponds to a wavelength of 365 nm. The ultrasonic irradiation was produced by using a high intensity sonificator at 20 kHz and 750 W power (Vibra Cell Ultrasonic Processor), with a probe of 13 mm diameter.

1 g/L of synthesized TiO_2-Mt as photocatalyst was added to 50 mg/L solution of the dye (DY106 and DV1). The resulting suspension was homogenized by stirring to reach the adsorption equilibrium of the dyes on the surface of the photocatalyst in dark condition before exposing to the light, the ultrasound or coupling of them.

The decomposition of DY106 and DV1 dyes were examined for analytical samples withdrawn from the photo-reactor at regular time intervals of 15 min. The samples were further centrifuged at 5000 rpm for 10 min and analyzed using UV-Visible spectrophotometer. Comparative tests were performed with TiO_2-P25 Degussa as a commercial catalyst; the effect of the calcination mode of TiO_2-Mt (microwaves and oven), as well as the effect of the pH of the colored solution were also studied.

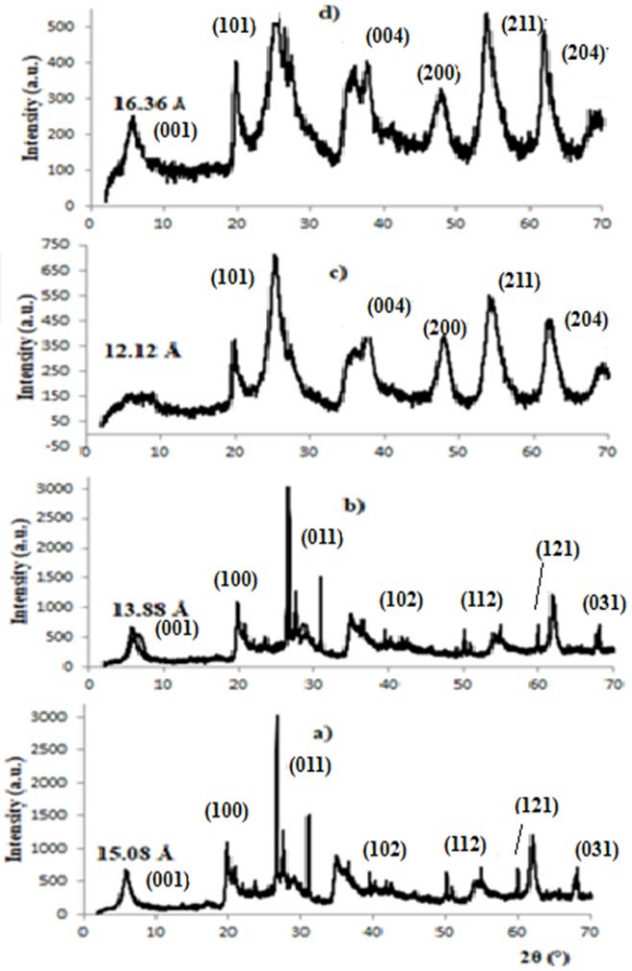

Figure 1. X-Ray diffraction patterns of a) Bentonite, b) Na-Mt (reference N°. 46-1045 for Quartz), c) TiO_2-Mt/oven and d) TiO_2-Mt/MW (reference JCPDS No. 73-1764 for Anatase phase) and Réflexion (001) of Mt.

3. Results and Discussions

3.1 Characterization of the Photocatalysts

TiO_2-Mont is the pillared clay, modified by intercalation of TiO_2 between the clay sheets. These clays have significantly better properties than base clay: high thermal stability, large pore opening, large specific surface, better adsorptive properties and significant catalytic activity. After adsorption of the dye molecules and their attachment to the TiO_2 pillars, they will be degraded by activation of the TiO_2-Mont particle, irradiation by ultraviolet radiation in the presence of ultrasonic waves.

Figure 1 illustrates the XRD patterns of the raw bentonite, the modified clay and the synthesized TiO_2/Mt over a $2 \leq 2\theta \leq 50$ angular range. The basal distance of the natural clay is 15.08 Å ($2\theta = 5.8°$), while it is 13.88 Å for the Na-Mt ($2\theta = 6.5°$), due to purification using NaCl, it is 16.36 Å for TiO_2-Mt/MW indicating the efficiency of the intercalation of TiO_2 within montmorillonite and 12.12 Å for TiO_2-Mt/oven, thus the presence of peak of montmorillonite localized at $2\theta = 20°$ for precursor and Pillared clays.

The diffraction peaks 2θ of 21°, 26.5°, 39.4°, 50°, 60° and 68° are attributed to the quartz phase of the clay, as well as the peaks where similar characteristics were observed for Na-Mt. Moreover, the XRD pattern of TiO_2-Mt demonstrated a characteristic diffraction peak at 2θ of 25.2°, 37°, 38°, 48°, 55° and 63°, indicating the presence of anatase phase [41-46], which were noted at the same diffraction peaks angle positions in the XRD pattern of TiO_2-P25 [47-48].

Table 2 shows the chemical composition analysis of the raw bentonite, sodium montmo-

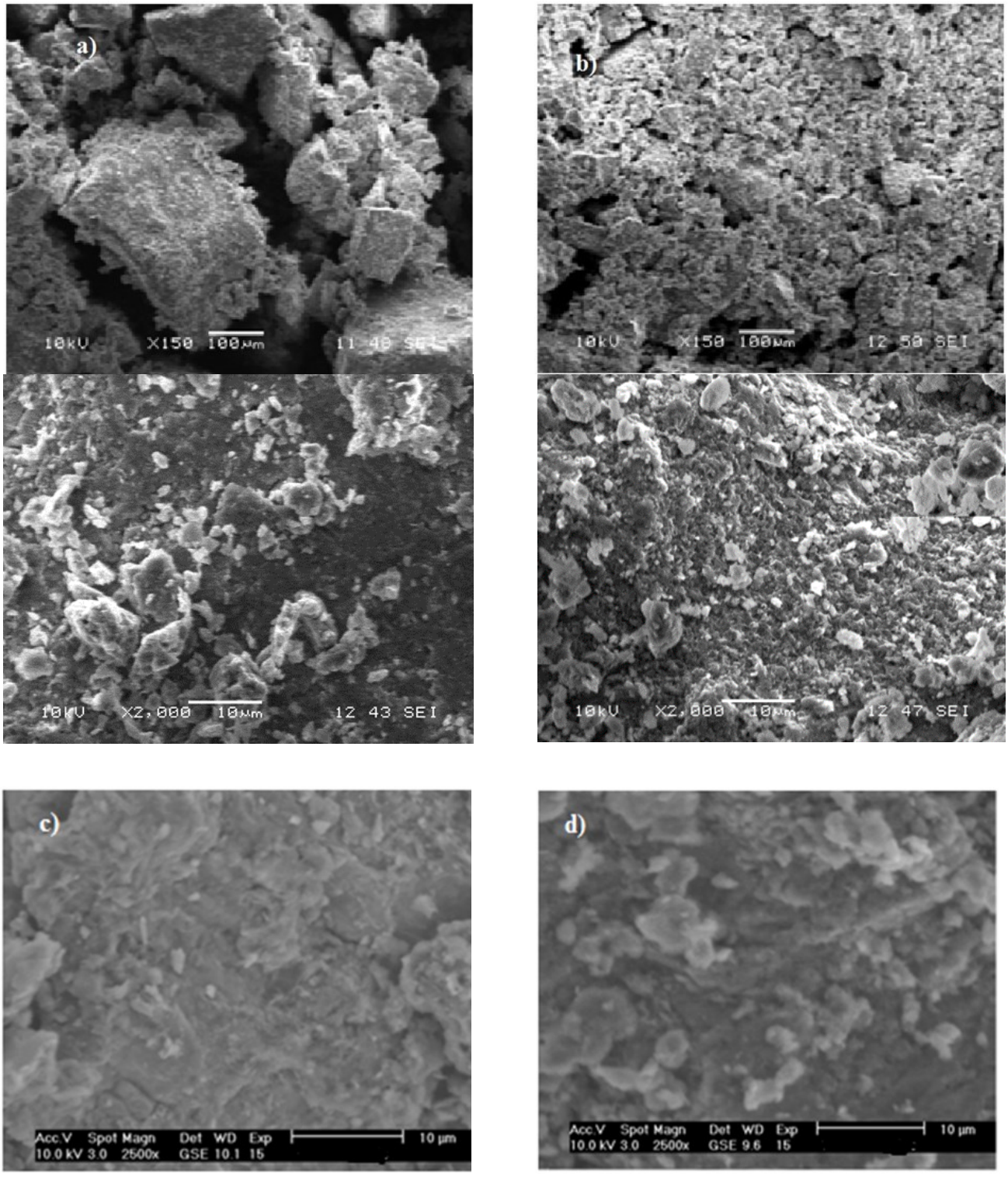

Figure 2. SEM image of photocatalysts, a) TiO_2-Mt/oven and b) TiO_2-Mt/MW (images taken at 150X and 2000X magnification), c) Bentonite and d) Na-Mt.

rillonite (Na-Mt), intercalated montmorillonite (TiO_2-Mt) and TiO_2-P25 Degussa. The major components contained in the raw bentonite and Na-Mt is SiO_2, followed by Al_2O_3, while the titanium oxide does not exceed 0.28%. Meanwhile the TiO_2 content in TiO_2-Mt/MW and TiO_2-Mt/oven was higher, of the order of 48.80% and 46.10%, respectively, which confirm the insertion of the polycation. This percentage reaches almost 100% (99.52%) in TiO_2-P25 Degussa.

Figure 2 shows SEM images of the pillared samples TiO_2-Mt/oven, TiO_2-Mt/MW, bentonite and Na-Mt. Small aggregated TiO_2 particles are dispersed on the flat plates and the interlayer space of the hydrophobic and pillared montmorillonite, with different shapes and sizes are clearly seen. Thus, the SEM images for these pillared clays indicated that the plate-like structure was substantially altered upon intercalation by the Ti-polycation. The SEM analysis represents the morphology, the textural aspect of clays and pillared clays. All micrograph present aggregates; in the case of Na-Mt, shows larger aggregates of particles that are closer to each other. For TiO_2-Mt/oven and TiO_2-Mt/MW, it is clearly seen that the agglomerates of titanium particles are well dispersed on the surface of the clay, leading to a regular and orderly morphology, confirming the good insertion of TiO_2 in the interlayer space of clay.

The results obtained from the BET analysis show an increase in the specific surface area, due to the purification and the cationic exchange with the Na^+ ion, as well as the intercalation of the titanium polycation. It is equal to 41.57 m^2/g, 162.54 m^2/g, 221.40 m^2/g, 233.67 m^2/g and 54.57 m^2/g for bentonite, Na-Mt, TiO_2-Mt/oven, TiO_2-Mt/MW and TiO_2-P25 Degussa, respectively. The thermograms (DTA) (Figure 3) of the two pillared clays (TiO_2-Mt/MW and TiO_2-Mt/oven) have several endothermic and exothermic effects. The first endothermic peak located around 100 °C, is quite intense and clearly visible in both samples; it reflects the loss of moisture hygroscopic water (dehydration) and shows the hydrophilic nature of these materials. The endothermic peaks of weak intensities that extend from 450 to 600 °C correspond to the dehydroxylation of bridged clays [49].

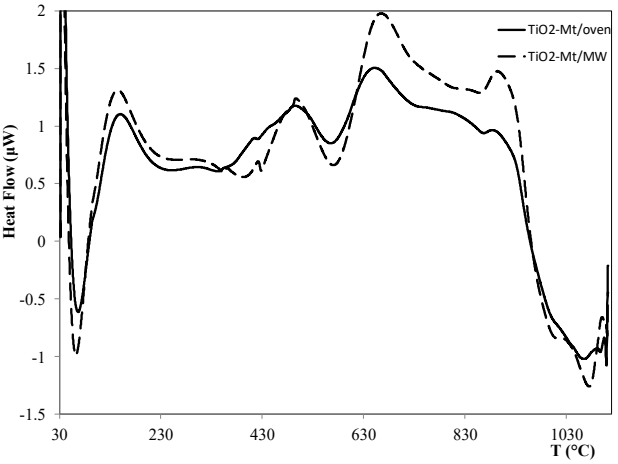

Figure 3. DTA curves of photocatalysts.

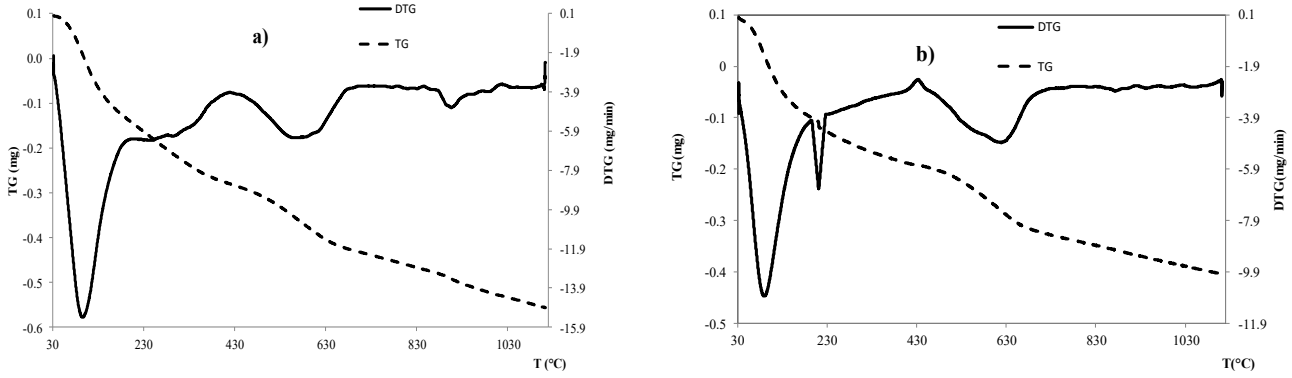

Figure 4. TG and DTG curves of photocatalysts, a) TiO_2-Mt/oven and b) TiO_2-Mt/MW.

Table 2. Chemical composition of bent, Na-Mt, TiO_2-Mt/oven, and TiO_2-Mt/MW samples.

Samples/Oxides (%)	Al_2O_3	SiO_2	Na_2O	MgO	K_2O	CaO	TiO_2	Fe_2O_3
Bent	19.01	66.97	1.13	3.95	2.56	0.85	0.21	3.98
Na-Mt	17.24	66.10	2.75	3.92	2.95	1.23	0.28	4.24
TiO_2-Mt/MW	11.78	34.37	-	2.11	0.51	0.99	48.80	1.92
TiO_2-Mt/oven	12.05	34.89	-	2.25	0.57	0.99	46.10	2.00

The peak of obvious exothermic nature located around 940–950 °C is due to the destruction and recrystallization of the silicate network. It confirms the thermal stability of these silicate materials and suggests their possible use at high temperatures. The exothermic peaks around 425 °C, average TiO_2-Mt/oven intensities, and relatively low TiO_2-Mt/MW correspond to the formation of the anatase phase [50]. The profile of the two thermogravimetric TG and DTG (Figure 4(a) and (b)) curves are virtually identical for both photocatalysts. It shows a loss of first mass starting from 100 °C, followed by progressive losses between 400 °C and 550 °C, then light up to about 1100 °C. The remarkable weight losses occurred in two stages: 100 °C and 400-670 °C. The first step is the loss of physically adsorbed water, while the second is attributed to the dehydroxylation of the clay structure and the elimination of the remaining hydroxide groups from the pillars and even the transformation of the pillars into to crystalline TiO_2 [51].

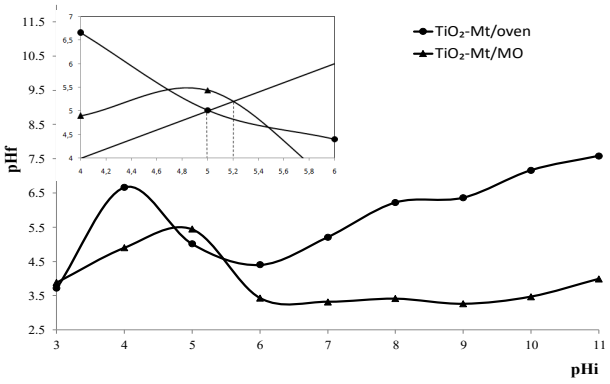

Figure 5. Plot for the determination of pH_{pzc}

These curves thus confirmed a good thermal stability of the pillar clays, the total loss in weight is about 7.7% and 12.7% attributing to TiO_2-Mt/oven and TiO_2-Mt/MW, respectively. According to the point of zero charge analysis (Figure 5), the pH_{pzc} of the surface of TiO_2-Mt/MW is 5.2 and 5 for TiO_2-Mt/oven. Therefore, the TiO_2-Mt surface has positive charge at pH_s lower than pH_{pzc} and negative charge at pH_s higher than. Thus, at pH values near the pH_{pzc}, the neutral dye molecules can be adsorbed on the overall non-charged TiO_2-Mt surface owing to intermolecular interactions.

3.2 Adsorption Experiments

The adsorption results of the dyes have been illustrated in Figure 6 (a) and (b). The adsorption capacity of the DV1 reached equilibrium at 105 min was 19.3% and 34% for TiO_2-Mt/oven and TiO_2-Mt/MW, respectively. Meanwhile, it was 25.6% for DY106 at 105 min with TiO_2-Mt/MW, but the adsorption capacity of it in the presence of TiO_2-Mt/oven is only 2% at 15 min approximately.

The azo dye DY106 is weakly adsorbed compared to the anthraquinone dye DV1 and in addition, the adsorption on TiO_2-Mt calcined under microwave is greater than that calcined in the oven. This adsorption capacity of TiO_2-Mt calcined under microwave compared with that calcined in the oven, it is related to the width of the range of the PZC field from pH 2.5 to pH 6, by that obtained by the conventional method varies from pH 2.5 to 4.5. From these adsorption results, it can be deduced that the DV1 anthraquinone dye is in its positively charged dissociated form (cationic form) and that the azo

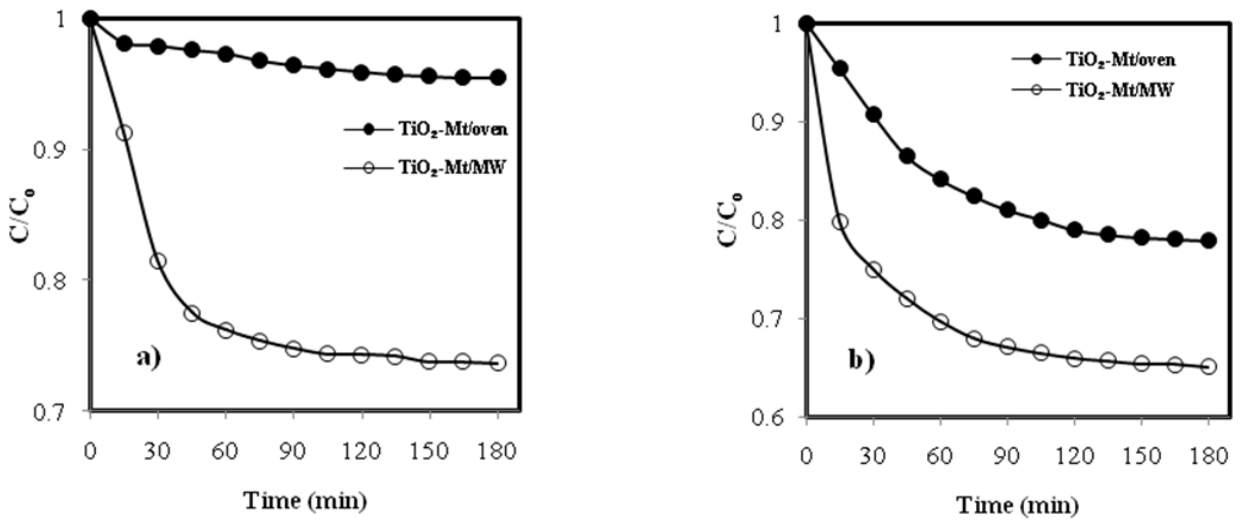

Figure 6. Adsorption profile of a) DY106 and b) DV1: [TiO_2-Mt] = 1 g/L, [Dye] = 50 mg/L, T = 19±1 °C, pH = 6.3.

dye DY106 exists mainly in anionic form of the same charge as the photocatalysts.

The adsorption of the dye molecules present in solution on TiO_2-Mont is done by physical (electrostatic) adsorption as a function of time and is carried out in several steps: (a) transport of the dye molecules in solution to the limit layer surrounding the particle from TiO_2-Mont; (b) transport of the dye molecules through the limit layer to the outside of the TiO_2-Mont particle; (c) diffusion of dye molecules inside the pores; (d) physisorption of dye molecules on the internal surface (adsorption sites) of TiO_2-Mont. The degradation of the molecules takes place after the adsorption step, since the latter corresponds to the fixation of the molecules, it is due to electrostatic forces between the colored solution and the surface of the solid, involving low energies; thus leaving in turn the other molecules present in solution to follow the same fate.

A relationship between the surface charge of the catalyst and that of the dye is established during adsorption. The zero charge point of TiO_2 is 5.3, therefore, the surface of TiO_2-Mont is positively charged in acidic medium while it is negatively charged in basic medium. Thus at pH 4, the electrostatic attraction of the positively charged catalyst results in a strong adsorption of the dye (considerable adsorption rate) which in turn is negatively charged. TiO_2-Mont behaves like a strong Lewis acid and, on the other hand, the dye acts like a strong Lewis base.

On the other hand, at basic pH, there is adsorption of hydroxide anions instead of the dye molecules leading to neutralization of the charge of the catalyst.

3.3 Photolysis, Sonolysis, and Sonophotolysis Experiments

We note that the behavior of the two dyes (azo and anthraquinone) is virtually similar throughout the processes mentioned previously for DY106 and DV1. Before sonocatalytic, photocatalytic, and sonophotocatalytic processes, photolysis, sonolysis, and sonophotolysis were investigated (Figure 7(a) and (b)), the aqueous solution of dyes was exposed to ultrasound or lamp irradiation and the change of dye concentration was monitored using UV-VIS spectrophotometer. The photolysis and sonolysis processes as well as their couplings in the absence of the photocatalysts, consists in the irradiation of the colored solution to be treated, by a UV radiation or submission of this one to the ultrasound or to the coupling of the two, show the stability of the two dyes with respect to the UV rays and the ultrasounds.

In the photolysis (8.4% and 0.5%) and sonolysis (10% and 6%) processes, no observed decrease in C/C_o with respect to irradiation time, indicating that there is no discoloration of DY106 and DV1, respectively. However, their coupling in the absence of photocatalysts has led to an elimination of 20% and 30% for the anthraquinone dye DV1 and the azo dye DY106, respectively, due to the presence of the hydroxyl radicals obtained by the cavitation phenomenon and those derived from UV rays photolysis process.

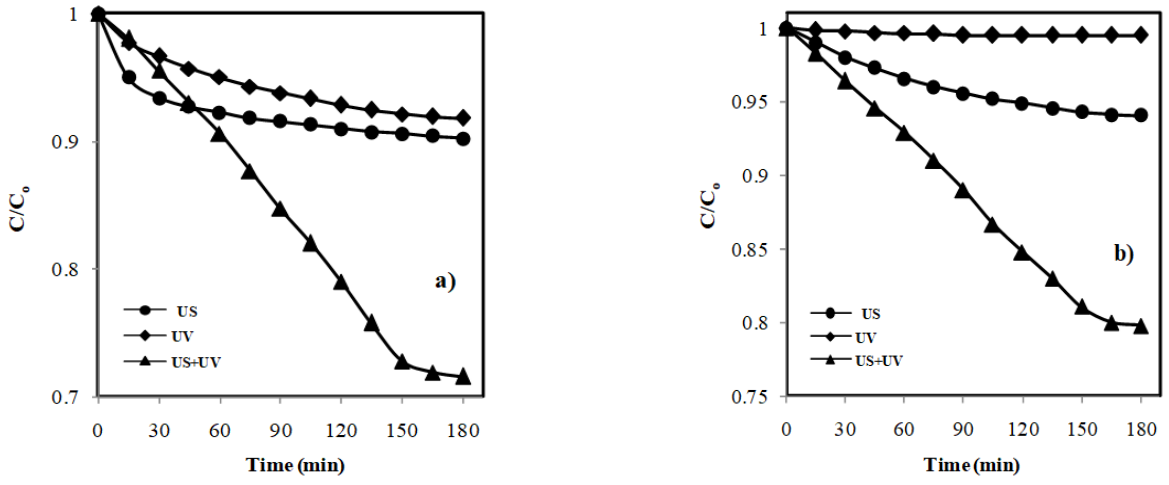

Figure 7. Degradation of a) DY106 and b) DV1 by photolysis (UV), sonolysis (US), and sonophotolysis (US+UV) processes: [Dye] = 50 mg/L, T = 19±1 °C, pH= 6.3.

3.4 Effect of Calcinations Mode in Photocatalysis, Sonocatalysis, and Sonophotocatalysis Experiments

A concentration of TiO_2-Mt (1 g/L) is contacted with 50 mg/L of dye solution (DY106 or DV1) for degrading by sonocatalytic and photocatalytic processes. However, the sonocatalytic degradation (US + TiO_2-Mt) of the dyes is slower, with medium rate, while under photocatalysis process (UV + TiO_2-Mt), the degradation occurred at a relatively high rate. The results obtained are shown in Figure 8(a), (b), (c), and (d). The TiO_2-Mt/oven photocatalyst has a low activity, during the photocatalytic, sonocatalytic, and sonophotocatalytic processes, compared to TiO_2-Mt/MW, it was 28.2% and 40.3% (US + TiO_2-Mt/oven), 33% and 48% (UV + TiO_2-Mt/oven), 81% and 70% (US + UV + TiO_2-Mt/oven), 97% and 86% (US + UV + TiO_2-Mt/MW), opposite to 50% and 45% (US + TiO_2-Mt/MW), 60% and 70.3% (UV + TiO_2-Mt/MW), respectively for DY106 and DV1. The calcination in the oven is heterogeneous whatever the calcined medium, in which the phenomenon is slow and tends toward thermal equilibrium. It took about 100 min to reach the desired calcination temperature 400 °C, while it is homogeneous under microwave, based on the direct absorption of energy by the product. The temperature can become stronger in the core of the material than on its surface, which accelerates the internal evaporation [52].

The photocatalytic tests carried out with photocatalysts calcined under microwave are more efficient than their counterparts calcined in the oven under UV irradiations or under ultrasound and the results obtained under UV irradiation are better for the two dyes studied. However, the degradation rate for the DY106

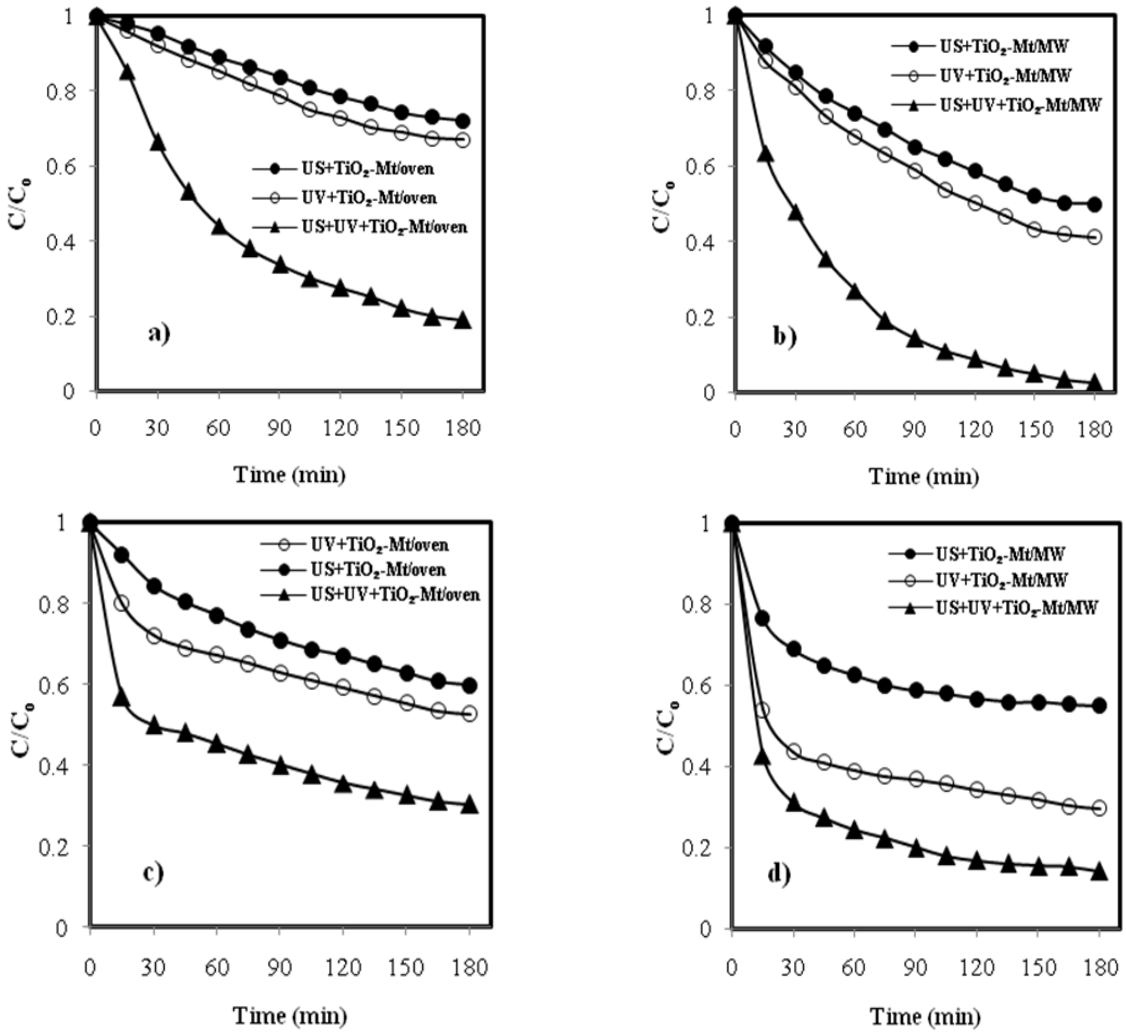

Figure 8. Effect of calcinations mode in photocatalytic (UV), sonocatalytic (US), and sonophotocatalytic (US+UV) degradation of DY106 (a,b) and DV1 (c,d) in presence of TiO_2-Mt/oven and TiO_2-Mt/MW respectively: [TiO_2-Mt] = 1 g/L, [Dye] = 50 mg/L, T = 19±1 °C, pH = 6.3.

dye is higher. These results show the importance of hydroxyl radicals through UV irradiation which are largely efficient than those produced during the implosion of air bubbles during the phenomenon of cavitation.

According to the results obtained previously, the sonophotocatalytic tests performed with the coupling of ultrasound with UV irradiation, especially in the case of the photocatalyst prepared during the calcination by microwave, allow an almost total elimination of the dyes after 3 hours, particularly for the DY106 azo dye. This selectivity for the degradation of this azo dye is due to molecular form characterized by its low ionization rate.

Given the best activity of TiO_2-Mt/MW, we have chosen to continue its application in this study. In the sonophotocatalytic process, the TiO_2-Mt is irradiated by ultraviolet radiation in the presence of ultrasonic waves. This combination offers a synergistic effect which increases the rate of degradation of the dyes, due to highly reactive free radicals. The latter are generated consecutively by the electron-hole pairs created by the excitation of TiO_2-Mt particles by ultraviolet radiation and by the action of ultrasound, thus increasing their concentration in solution; therefore creating the synergistic effect in sonophotocatalysis.

On the other hand, the improvement in degradation can also be explained by the increase in mass transport of chemical species between the solution phase and the surface of the catalyst and, the additional yields of OH• radicals by acoustic cavitation. In addition, the continuous cleaning of the surface of TiO_2-Mt by acoustic cavitation could also play a role in the modification of the photocatalytic speed, so the use of ultrasound creates conditions of increased turbulence in the liquid, thus reducing the limits of mass transfer and increases the specific surface and therefore the catalytic performance.

The photoexcitation of Mont-TiO_2 occurs by the absorption of a photon of wavelength ≤ 365 nm creating electron-hole pairs. The electron in the conduction band is available for reduction and the hole in the valence band is available for oxidation. The hole then reacts by electron transfer with the adsorbed water to form a radical species which is the hydroxyl radical OH•, similarly produced by acoustic cavitation (sonolysis of water), which is a powerful oxidant, attacks the compounds organic (dye molecules) and intermediate compounds. These intermediates also react with hydroxyl radicals to give final products.

$$TiO_2\text{-}Mont \xrightarrow{hv} TiO_2\text{-}Mont + h^+_{bv} + e^-_{bc} \quad (3)$$

$$hv^+_{bv} + e^-_{bc} \longrightarrow heat \quad (4)$$

$$H_2O_{ads} + h^+_{bv} \longrightarrow OH\bullet_{ads} + H^+ \quad (5)$$

$$H_2O \xrightarrow{))))} OH\bullet_{ads} + H\bullet \quad (6)$$

$$TiO_2\text{-}Mont + Dye \longrightarrow Dye_{ads} \quad (7)$$

$$Dye_{ads} + OH\bullet_{ads} \longrightarrow Intermediates \quad (8)$$

$$Intermediates + OH\bullet_{ads} \rightarrow Final\ product \rightarrow H_2O + CO_2 \quad (9)$$

3.5 Comparative Study Between TiO_2-Mt/MW and TiO_2-P25 Degussa in Sonophotocatalysis Experiments

For comparison, the behavior of TiO_2-P25 (0.5 g/L) was also investigated as a reference under the same conditions for sonophotocatalytic degradation. The sonophotocatalytic degradation of the two dyes has reached the maximum rate of decolonization when compared with the sonocatalytic and photocatalytic processes, (US + UV + TiO_2-Mt/MW) and (US + UV + TiO_2). TiO_2-Mt/MW has a pH_{pzc} equal to 5.2, a value close to that of the commercial TiO_2 (5.3), resulting that their behavior is however similar (Figure 9(a) and (b)), the decoloration rate reaches 97% for TiO_2-Mt/MW and TiO_2-P25, (86% and 70%) after 3 hours of reaction for DY106 and DV1, respectively. Therefore, the results confirm the effectiveness and the good activity of the photocatalyst TiO_2-Mt/MW.

In addition, the presence of ultrasound enhances the interaction of dyes (DY106 and DV1) with the electronic charges generated during the catalytic process (presence of TiO_2-Mt). Therefore the maximum charge carrier was achieved during the sonophotocatalytic degradation of dyes. In the sonophotocatalysis, the ultrasonic waves act on the whole volume of the photocatalyst, the whole mass of the latter participates in the oxidation reaction, so the synergistic effect of UV and ultrasound generates a higher local concentration of reactive species, in particular hydroxyl radical (OH•) [53], the hydrogen (H•) radicals followed by hydroperoxyl radicals ($HO•_2$) and hydrogen peroxide are generated [1].

Thus, this increase in the production of hydroxyl radicals in the reaction mixture is followed by an improved mass transfer of organic substances between the liquid phase and the catalyst surface and by an excitation of the latter by luminescence induced by ultrasound

which has a wide range of wavelengths below 375 nm. This phenomenon leads to increase in the catalytic activity of the photocatalyst. Finally, a cleaning and a sweeping of the catalyst surface due to the acoustic micro-diffusion allows more active catalyst sites to be available for the reaction [22], which concluded the beneficial effect of the coupling photocatalysis with sonolysis.

3.6 Effect of pH Solution in Sonophotocatalysis Experiments

The pH plays an important role in the sonophotocatalytic degradation of colored solutions, it was adjusted by adding 0.1 N HCl or 0.1 N NaOH. The effect of the three pH (4, 6.3 and 10), is illustrated in Figure 10, representing the variation of the C/C_0 as a function of time, revealing a better performance of the sonophotocatalytic degradation which is obtained in acid medium (pH = 4). The influence of pH on the removal rate is intimately related to the photocatalyst PZC and therefore, the best degradation rate is in the region just above the PZC, but also prevents the interference of the cationic forms of the dyes with the hydroxide anions of the basic medium.

The degradation rate reaches the maximum (100%) for 3 hours of reaction, in the acidic medium, resulting from the electrostatic attraction of the positively charged photocatalyst and the ionized dye, followed by the pH of the solution, then a decrease of this rate to pH = 10. At this pH, the molecules of the anionic dye move

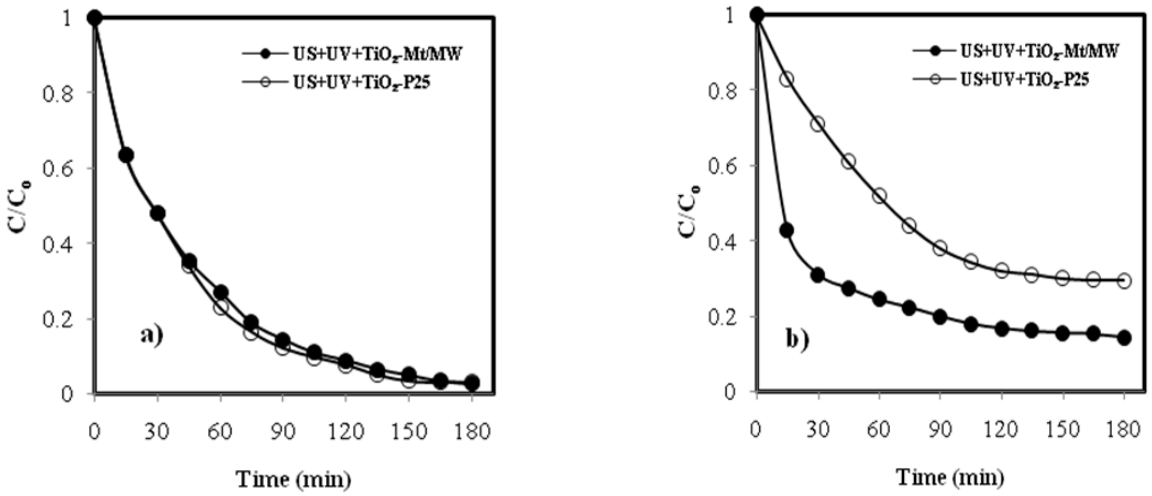

Figure 9. Sonophotocatalytic degradation of a) DY106 and b) DV1: effect TiO_2-Mt/MW and TiO_2-P25 Degussa: [TiO_2-Mt/MW] = 1 g/L, [TiO_2-P25] = 0.5 g/L, [Dye] = 50 mg/L, T = 19±1 °C, pH = 6.3.

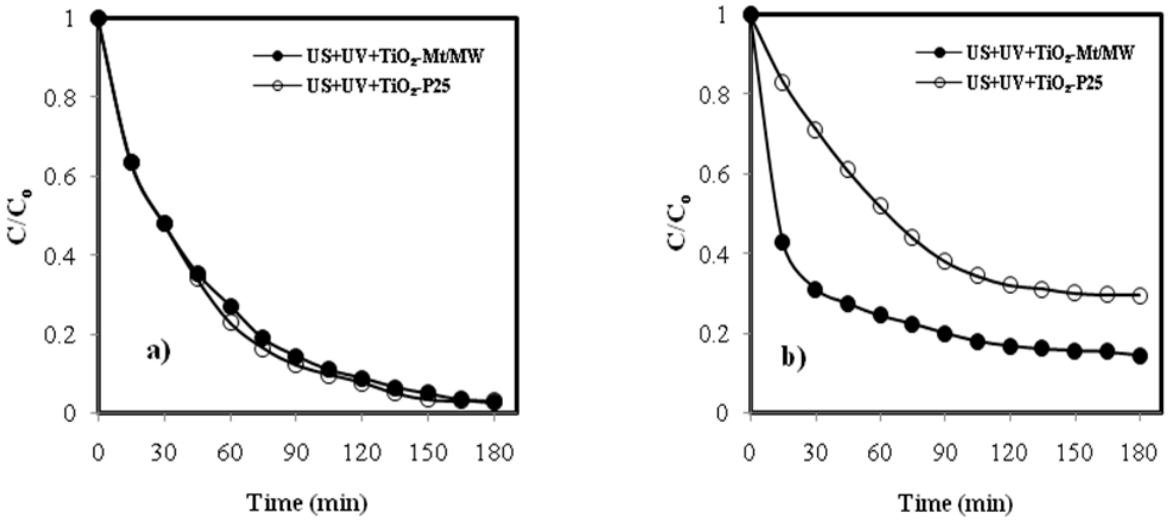

Figure 10. Effect of pH solution in sonophotocatalytic degradation of a) DY106 and b) DV1: [TiO_2-Mt/MW] = 1 g/L, [Dye] = 50 mg/L, T = 19±1 °C.

away from the negatively charged photocatalyst surface [54]. TiO_2-Mont/MW has a pH_{pzc} equal to 5.2 (pH < 5.2). Mahmoodi and Arami [55] confirmed that when the pH of the polluted solution is lower than the pH_{pzc}. Its surface is positively charged in an acid medium, resulting an electrostatic attraction between the positively charged surface of photocatalyst and anionic dyes. Meanwhile, with increasing pH of the reaction medium, the number of negatively charged sites increases, thereby creating electrostatic repulsion.

In the sonophotocatalysis, the OH• radicals are in a high rate compared to photocalytic or sonocatalytic processes. At low pH values (acidic pH), the dye molecules are at the bubble interface, with higher concentrations to OH•, thus able to penetrate the cavitations bubbles, since they are essentially in their neutral form [14].

4. Conclusion

In this study, the experimental results showed that the characterization of TiO_2-Mt nanoparticules by XRD, XRF, BET, SEM, TG/DTA and pH_{pzc} analyses confirmed the intercalation of TiO_2 in montmorillonite, while the calcination with microwave is more efficient, allowing the acquisition of a better activity to the photocatalyst.

The TiO_2-Mt photocatalysts were successfully used for sonophotocatalytic degradation of dyes DY106 (azo) and DV1 (anthraquinone) in aqueous media, where the rate of degradation was slow by sonolysis and photolysis. Meanwhile, the presence of photocatalyst improved the removal rate of both dyes. It was clearly better in the case of photocatalysis compared to obtained with sonocatalysis process, proving the effectiveness of the microwave calcination method. Meanwhile, a strong synergy was observed by the coupling of UV, US and TiO_2-Mt/MW (sonophotocatalytic process), which proves the high catalytic activity of the photocatalyst and a better degradation obtained in acid medium followed by the pH of the solution.

Acknowledgement

This work was carried with the financial support of the Direction Générale de la Recherche Scientifique et du Développement Technologique (DGRSDT)/Ministère de l'Enseignement Supérieur et de la recherche Scientifique d'Algérie (MESRS).

References

[1] Markovic, D., Aponjic, Z.S., Radoicic, M., Radetic, T., Vodnik, V., Potkonjak, B., Radetic, M. (2015). Sonophotocatalytic degradation of dye C.I. Acid Orange 7 by TiO_2 and Ag nanoparticles immobilized on corona pretreated polypropylene non-woven fabric. *Ultrasonics Sonochemistry*, 24, 221–229. DOI: 10.1016/j.ultsonch.2014.11.017.

[2] Gole, V.L., Gogate, P.R. (2014). Degradation of brilliant green dye using combined treatment strategies based on different irradiations. *Separation and Purification Technology*, 133, 121–220. DOI: 10.1016/j.seppur.2014.07.002.

[3] Khan, M.A.N., Siddique, M., Wahid, F., Khan, R. (2015) .Removal of reactive blue 19 dye by sono, photo and sonophotocatalytic oxidation using visible light. *Ultrasonics Sonochemistry*, 26, 370–377. DOI: 10.1016/j.ultsonch.2015.04.012.

[4] Dukkanci, M., Vinatoru, M., Mason, T.J. (2014). The sonochemical decolourisation of textile azo dye Orange II: Effects of Fenton type reagents and UV light. *Ultrasonics Sonochemistry*, 21, 846–853. DOI: 10.1016/j.ultsonch.2013.08.020.

[5] Basturk, E., Karatas, M. (2015). Decolorization of antraquinone dye Reactive Blue 181 solution by UV/ H_2O_2 process. *Journal of Photochemistry and Photobiology A: Chemistry*, 299, 67–72. DOI: 10.1016/j.jphotochem.2014.11.003.

[6] He, Z., Lin, L., Song, S., Xia, M., Xu, L., Ying, H., Chen, J. (2008). Mineralization of C.I. Reactive Blue 19 by ozonation combined with sonolysis: Performance optimization and degradation mechanism. *Separation and Purification Technology*, 62, 376–38. DOI: 10.1016/j.seppur.2008.02.005.

[7] Mosleh, S., Rahimi, M.R., Ghaedi, M., Dashtian, K. (2016). Sonophotocatalytic degradation of trypan blue and vesuvine dyes in the presence of blue light photocatalyst of Ag_3PO_4/Bi_2S_3-HKUST-1-MOF: Central composite optimization and synergistic effect study. *Ultrasonics Sonochemistry*, 39, 676–68. DOI: 10.1016/j.ultsonch.2016.04.007.

[8] Monteagudo, J.M., Duran, A., San Martin, I., Garcia, S. (2014). Ultrasound-assisted homogeneous photocatalytic degradation of Reactive Blue 4 in aqueous solution. *Applied Catalysis B: Environmental*, 152–153, 59–67. DOI : 10.1016/j.apcatb.2014.01.014.

[9] Sun, J.H., Sun, S.P., Sun, J.Y., Sun, R.X., Qiao, L.P., Guo, H.Q., Fan, M.H. (2007). Degradation of azo dye Acid black 1 using low concentration iron of Fenton process facilitated

by ultrasonic irradiation. *Ultrasonics Sonochemistry*, 14, 761–766. DOI: 10.1016/j.ultsonch.2006.12.010.

[10] Kumar, R., Kuma, G., Akhtar, M.S., Umar, A. (2015). Sonophotocatalytic degradation of methyl orange using ZnO nano-aggregates. *Journal of Alloys and Compounds*, 629, 67–172. DOI: 10.1016/j.jallcom.2014.12.232.

[11] Ahmad, M., Ahmed, E., Hong, Z.L., Ahmed, W., Elhissi, A., Khalid, N.R. (2014). Photocatalytic, sonocatalytic and sonophotocatalytic degradation of Rhodamine B using ZnO/CNTs composites photocatalysts. *Ultrasonics Sonochemistry*, 21, 761–773. DOI: 10.1016/j.ultsonch.2013.08.014.

[12] Lops, C., Ancona, A., Cesare, K.D., Dumontel, B., Garino, N., Canavese, G., Hérnandez, S., Cauda, V. (2019). Sonophotocatalytic degradation mechanisms of Rhodamine B dye via radicals generation by micro- and nanoparticles of ZnO. *Applied Catalysis B: Environmental*, 243, 629–640. DOI: 10.1016/j.apcatb.2018.10.078.

[13] Panahian, Y., Arsalani, N., Nasiri, R. (2018). Enhanced photo and sono-photo degradation of crystal violet dye in aqueous solution by 3D flower like F-TiO_2(B)/fullerene under visible light. *Journal of Photochemistry and Photobiology A: Chemistry*, 365, 45–51. DOI: 10.1016/j.jphotochem.2018.07.035.

[14] Ertugay, N., Acar, F.N. (2014). The degradation of Direct Blue 71 by sono, photo and sonophotocatalytic oxidation in the presence of ZnO nanocatalyst. *Applied Surface Science*, 318, 121–126. DOI: 10.1016/j.apsusc.2014.01.178.

[15] Karaca, M., Kıransan, M., Karaca, S., Khataee, A., Karimi, A. (2016). Sonocatalytic removal of naproxen by synthesized zinc oxide nanoparticles on montmorillonite. *Ultrasonics Sonochemistry*, 31, 250–256. DOI: 10.1016/j.ultsonch.2016.01.009.

[16] Gonzalez, S., Martinez, S.S. (2008). Study of the sonophotocatalytic degradation of basic blue 9 industrial textile dye over slurry titanium dioxide and influencing factors. *Ultrasonics Sonochemistry*, 15, 1038–1042. DOI: 10.1016/j.ultsonch.2008.03.008.

[17] Zhou, M., Yang, H., Xian, T., Li, S., Zhang, H.M., Wang, X.X. (2015). Sonocatalytic degradation of RhB over $LuFeO_3$ particles under ultrasonic irradiation. *Journal of Hazardous Materials*. 289, 149–157. DOI: 10.1016/j.jhazmat.2015.02.054.

[18] Ghoreishian, S.M., Raju, G.S.R., Cheol, E.P., Kwak, H., Han, Y.K., Huh, Y.S. (2019). Ultrasound-assiste heterogeneous degradation of tetracycline over flowerlike rGO/CdWO4 hierarchical structures as robust solar-light-responsive photocatalysts: Optimization, kinetics, and mechanism. *Applied Surface Science*, 489, 110–122. DOI: 10.1016/j.apsusc.2019.05.299.

[19] He, Y., Grieser, F., Ashokkumar, M. (2011). The mechanism of sonophotocatalytic degradation of methyl orange and its products in aqueous solutions. *Ultrasonics Sonochemistry*, 18, 974–980. DOI: 10.1016/j.ultsonch.2011.03.017.

[20] Bejarano-Perèz, N.J., Suarèz-Herrera, M.F. (2008). Sonochemical and sonophotocatalytic degradation of malachite green: The effect of carbon tetrachloride on reaction rates. *Ultrasonics Sonochemistry*, 15(4), 612–617. DOI: 10.1016/j.ultsonch.2007.09.009.

[21] Madhavan, J., Kumar, P.S.S., Anandan, S., Grieser, F., Ashokkumar, M. (2010). Degradation of acid red 88 by the combination of sonolysis and photocatalysis. *Separation and Purification Technology*, 74, 336–341. DOI: 10.1016/j.seppur.2010.07.001.

[22] Kritikos, D.E., Xekoukoulotakis, N.P., Psillakis, E., Mantzavinos, D. (2007). Photocatalytic degradation of reactive black 5 in aqueous solutions: Effect of operating conditions and coupling with ultrasound irradiation. *Water Research,* 41, 2236–2246. DOI: 10.1016/j.watres.2007.01.048.

[23] Mrowetz, M., Pirola, C., Selli, E. (2003). Degradation of organic water pollutants through sonophotocatalysis in the presence of TiO_2. *Ultrasonics Sonochemistry*, 10, 247–254. DOI: 10.1016/S13504177(03)00090-7.

[24] Wu, C.H., Yu, C.H. (2009). Effects of TiO_2 dosage, pH and temperature on decolorization of C.I. Reactive Red 2 in a UV/US/TiO_2 system. *Journal of Hazardous Materials*, 169, 1179–1183. DOI: 10.1016/j.jhazmat.2009.04.064.

[25] Cheng, Z., Quan, X., Xiong, Y., Yang, L., Huang, Y. (2012). Synergistic degradation of methyl orange in an ultrasound intensified photocatalytic reactor. *Ultrasonics Sonochemistry,* 19, 1027–1032. DOI: 10.1016/j.ultsonch.2012.02.008.

[26] Wang, H., Niu, J., Long, X., He, Y. (2008). Sonophotocatalytic degradation of methyl orange by nano-sized Ag/TiO_2 particles in aqueous solutions. *Ultrasonics Sonochemistry,* 15, 386–392. DOI: 10.1016/j.ultsonch.2007.09.011.

[27] Talebian, N., Nilforoushan, M.R., Mogaddas, F.J. (2013). Comparative study on the sonophotocatalytic degradation of hazardous waste. *Ceramics International,* 39(5), 4913–4921. DOI: 10.1016/j.ceramint.2012.11.085.

[28] Hossienzadeh, K., Maleki, A., Daraei, A., Safari, M., Pawar, R., Lee, S.M. (2019). Sonocatalytic and photocatalytic efficiency of transition metal-doped ZnO nanoparticles in the removal of organic dyes from aquatic environments. *Korean J. Chem. Eng.,* 36(8), 1360-1370. DOI: 10.1007/s11814-019-0299-6.

[29] Bokhale, N.B., Bomble, S.D., Dalbhanjan, R.R., Mahale, D.D., Hinge, S.P., Banerjee, B.S., Mohod, A.V., Gogate, P.R. (2014). Sonocatalytic and sonophotocatalytic degradation of rhodamine 6G containing Wastewaters. *Ultrasonics Sonochemistry*, 21, 1797−1804. DOI: 10.1016/j.ultsonch.2014.03.022.

[30] Kiransan, M., Khataee, A., Karaca, S., Sheydaei, M. (2015). Artificial neural network modeling of photocatalytic removal of a disperse dye using synthesized of ZnO nanoparticles on montmorillonite. *Spectrochimica Acta Part A: Molecular and Biomolecular Spectroscopy*, 140, 465−473. DOI: 10.1016/j.saa.2014.12.100.

[31] Hassani, A., Khataee, A., Karaca, S., Karaca, C., Gholami, P. (2017). Sonocatalytic degradation of ciprofloxacin using synthesized TiO_2 nanoparticles on montmorillonite. *Ultrasonics Sonochemistry,* 35(A), 251−262. DOI : 10.1016/j.ultsonch.2016.09.027.

[32] Taufik, A., Muzakkia, A., Saleh, R. (2018). Effect of nanographene platelets on adsorption and sonophotocatalytic performances of TiO_2/CuO composite for removal of organic pollutants. *Materials Research Bulletin*, 99, 109-123. DOI : 10.1016/j.materresbull.2017.10.033.

[33] Khalfaoui-Boutoumi, N., Boutoumi, H., Khalaf, H., David, B. (2013). Synthesis and characterization of TiO_2 Montmorillonite / Polythiophene-SDS nanocomposites: Application in the sonophotocatalytic degradation of rhodamine 6G. *Applied Clay Science*, 80(81), 56−62. DOI: 10.1016/j.clay.2013.06.005.

[34] Harrelkas, F., Paulo, A., Alves, M.M., El Khadir, L., Zahraa, O., Pons, M.N., Van der Zee, F.P. (2008). Photocatalytic and combined anaerobic–photocatalytic treatment of textile dyes. *Chemosphere*, 72, 1816−1822. DOI: 10.1016/j.chemosphere.2008.05.026.

[35] Damardji, B., Khalaf, H., Duclaux, L., David, B. (2009). Preparation of TiO_2-pillared montmorillonite as photocatalyst Part II. Photocatalytic degradation of a textile azo dye. *Applied Clay Science,* 45, 98−104. DOI: 10.1016/j.clay.2009.04.002.

[36] Xiuqin, O., Junping, M., Qimin, W., Junmei, Y. (2006). Enhanced Photoactivity of Layered Nanocomposite Materials Containing Rare Earths, Titanium Dioxide and Clay. *Journal of Rare Earths*, 24(Spec Issue), 251−254. DOI: 10.1016/S1002-0721(07)60373-1.

[37] Bouchenafa-Saïb, N., Khouli, K., Mohammedi, M. (2007). Preparation and characterization of pillared montmorillonite: Application in adsorption of cadmium. *Desalination,* 217, 282−290. DOI: 10.1016/j.desal.2007.03.007.

[38] Yingguang, L., Pihui, P., Dafeng, Z., Zhuoru, Y., Lianshi, W. (2010). Preparation and photocatalytic activity of laponite pillared by CeO_2 modified TiO_2. *Journal of Rare Earths*, 28(5), 32−36. DOI: 10.1016/S1002-0721(09)60190-3.

[39] Khalaf, H., Bouras, O., Perrichon, V. (1997). Synthesis and characterization of Al-pillared and cationic surfactant modified Al-pillared Algerian bentonite. *Microporous Materials*, 8, 141-150. DOI: 10.1016/S0927-6513(96)00079-X.

[40] Damardji, B., Khalaf, H., Duclaux, L., David, B, (2009). Preparation of TiO_2-pillared montmorillonite as photocatalyst Part I. Microwave calcination, characterisation, and adsorption of a textile azo dye. *Applied Clay Science*, 44, 201-205. DOI: 10.1016/j.clay.2008.12.010.

[41] Hassani, A., Khataee, A., Karaca, S. (2015). Photocatalytic degradation of ciprofloxacin by synthesized TiO_2 nanoparticles on montmorillonite: Effect of operation parameters and artificial neural network modeling. *Journal of Molecular Catalysis A: Chemical*, 409, 149−161. DOI: 10.1016/j.molcata.2015.08.020.

[42] Miao, S., Liu, Z., Han, B., Zhang, J., Yu, X., Du, J., Sun, Z. (2006). Synthesis and characterization of TiO_2-montmorillonite nanocomposites and their application for removal of methylene blue. *Journal of Materials Chemistry*, 16, 579−584. DOI: 10.1039/b511426h.

[43] Chen, D., Zhu, Q., Zhou, F., Deng, X., Li, F. (2012). Synthesis and photocatalytic performances of the TiO_2 pillared montmorillonite. *Journal of Hazardous Materials*, 235−236, 186−193. DOI: 10.1016/j.jhazmat.2012.07.038.

[44] Liu, J., Dong, M., Zuo, S., Yu, Y. (2009). Solvothermal preparation of TiO_2/montmorillonite and photocatalytic activity. *Applied Clay Science*, 43, 156–159. DOI: 10.1016/j.clay.2008.07.016.

[45] Belessi, V., Lambropoulou, D., Konstantinou, I., Katsoulidis, A., Pomonis, P., Petridis, D., Albanis, T. (2007). Structure and photocatalytic performance of TiO_2/clay nanocomposites for the degradation of dimethachlor. *Applied Catalysis B: Environmental*, 73, 292–299. DOI: 10.1016/j.apcatb.2006.12.011.

[46] Xu, Z., Xie, Q., Shuo, C., Hui-min, Z., Yu, L. (2007). Photocatalytic remediation of γ-hexachlorocyclohexane contaminated soils us-

ing TiO_2 and montmorillonite composite photocatalyst. *Journal of Environmental Sciences*, 19, 358–361. DOI: 10.1016/S1001-0742(07)60059-X.

[47] Liu, J., Li, X., Zuo, S., Yu, Y. (2007). Preparation and photocatalytic activity of silver and TiO_2 nanoparticles/montmorillonite composites. *Applied Clay Science*, 37, 275−280. DOI: 10.1016/j.clay.2007.01.008.

[48] Dong, F., Zhao, W., Wu, Z., Guo, S. (2009). Band structure and visible light photocatalytic activity of multi-type nitrogen doped TiO_2 nanoparticles prepared by thermal decomposition. *Journal of Hazardous Materials*, 162, 763–770. DOI: 10.1016/j.jhazmat.2008.05.099.

[49] Lenoble, V., Bouras, O., Deluchat, V., Serpaud, B., Bollinger, J.C. (2002). Arsenic Adsorption onto Pillared Clays and Iron Oxides. *Journal of Colloid and Interface Science*, 255, 52−58. DOI: https://doi.org/10.1006/jcis.2002.8646.

[50] Mogyorosi, K., Dekany, I., Fendler, .H. (2003). Preparation and Characterization of Clay Mineral Intercalated Titanium Dioxide Nanoparticles. *Langmuir,* 19, 2938−2946. DOI: 10.1021/la025969a.

[51] Valverde, J.L., De Lucas, A., Dorado, F., Sun-Kou, R., Sanchez, P., Asencio, I., Garrido, A., Romero, A. (2003). Characterization and Catalytic Properties of Titanium-Pillared Clays Prepared by Laboratory and Pilot Scales: A Comparative Study. *Ind. Eng. Chem. Res.*, 42, 2783−2790. DOI: 10.1021/ie0208772.

[52] Belmeskine, H., Kaemarerer, M., Andhuy, M., Khalaf, H. (2005). Cadmium removal from phosphate of Djebel Onk by thermal treatment. *Asian. J. Chem.,* 17(4), 2105−2116.

[53] Joseph, C.G., Puma, G.L., Bono, A., Krishnaiah, D., (2009). Sonophotocatalysis in advanced oxidation process: A short review. *Ultrasonics Sonochemistry*, 16, 583−589. DOI: 10.1016/j.ultsonch.2009.02.002.

[54] Kaur, S., Singh, V. (2007). Visible light induced sonophotocatalytic degradation of Reactive Red dye 198 using dye sensitized TiO_2. *Ultrasonics Sonochemistry,*14, 531–537. DOI: 10.1016/j.ultsonch.2006.09.015.

[55] Mahmoodi, N.M., Arami, M. (2009). Degradation and toxicity reduction of textile wastewater using immobilized titania nanophotocatalysis. *Journal of Photochemistry and Photobiology B: Bi*ology. 94, 20–24. DOI: 10.1016/j.jphotobiol.2008.09.004.